On the Resolution of the Synthetic-Aperture Passive Source Localization Algorithm

1st Andre Celestin
Institute for Telecommunication Sciences
National Telecommunications and Information Administration
Boulder, CO USA
acelestin@ntia.gov

2nd Matthew J Rhilinger
Institute for Telecommunication Sciences
National Telecommunications and Information Administration
Boulder, CO USA
mrhilinger@ntia.gov

3rd Margaret Cheney
Mathematics Department
Colorado State University
Fort Collins, CO USA
margaret.cheney@colostate.edu

***Abstract*—Source localization is the process of locating a source of electromagnetic waves or acoustic waves from passive measurements of the emitted fields made on distributed receivers. This is an important problem for both military and civilian applications. The Synthetic Aperture Passive Source Localization (SAPSL) algorithm combines statistical methods with techniques from Synthetic-Aperture Radar to attain a high-resolution image from two receivers. We focus on the case of wave propagation in a homogeneous medium, sources restricted to lie on a known surface, and slowly moving sensors. This paper contains resolution formulas for the SAPSL algorithm for two different sensor geometries. The first geometry consists of a stationary isotropic source located between one stationary sensor and one mobile sensor on a linear path. The second geometry consists of a stationary isotropic source and two mobile sensors following each other along a linear path. In both geometries, we make narrow-aperture assumptions in order to obtain simple resolution formulas. This paper also presents numerical simulations that verify the resolution predicted from the formulas.**

***Index Terms*—FDOA, geolocation, source localization, synthetic aperture, TDOA**

I. Introduction

Source Localization is the process of locating a source of electromagnetic waves or acoustic waves, using data received by passive receivers on known flight paths. The waves are assumed to be traveling through a homogeneous medium with speed c. For the sake of simplicity, the source is assumed to radiate isotropically. This problem has been studied in detail for decades because of its extensive uses in both civilian and military applications.

The problem consists of two parts: 1) detecting the presence of a common signal in data on two separate receivers and 2) locating the position of the source of that common signal. The statistical detection problem 1) has been studied in, *e.g.,* [1]–[6] in the case where the sources are modeled as transmitting unknown deterministic signals. This is also the signal model used in this paper. The localization problem 2) has been studied in the form of "two-step methods" in which time-difference-of-arrival (TDOA) and frequency-difference-of-arrival (FDOA) curves are computed, and then a system of nonlinear equations are solved to locate the source [7]. Direct position determination approaches, (*e.g.,* [8]) study both the statistical problem and the localization problem at once, using all of the data in a maximum likelihood estimation for the position of the source. The Synthetic Aperture Source Localization (SASL) algorithm developed by Waddington *et al*. [9], [10] applies a synthetic-aperture approach to cross-correlations of signals measured by two distinct sensor platforms. Waddington's approach, however, requires additional linearizing assumptions and does not involve statistics.

The SAPSL algorithm developed in [11] and discussed in this paper uses the generalized likelihood ratio (GLR) detection statistic developed in [6] along with Synthetic Aperture Radar (SAR) techniques to solve the passive source localization problem.

In this paper, a general overview of the SAPSL algorithm is discussed for the case in which the sensor positions are known and the system is perfectly synchronized in time. Resolution formulas for two sensor geometries of interest are presented. The first geometry consists of one stationary receiver, one mobile receiver following a straight line path, and an isotropic source positioned between the two receivers. The second geometry consists of two mobile sensors following each other in a straight line flight path with an isotropic and stationary source outside of the path. These geometries are assumed to be 2D, with the sensors and source positioned at the same altitude. Numerical simulations are presented that support the validity of the resolution formulas.

II. Imaging Algorithm

We consider a source, located at an unknown position $\boldsymbol{x}_0$, that is transmitting an unknown waveform of the form $\psi_{\boldsymbol{x}_0}(t) = \text{Re}\left[e^{i\omega_0 t} a_{\boldsymbol{x}_0}(t)\right]$. Here, $\omega_0 = 2\pi f_0$ is the angular carrier frequency for the transmitted complex baseband signal $a_{\boldsymbol{x}_0}(t)$. We model the transmission of electromagnetic waves with the scalar wave equation

$$\left(\nabla^2 - \frac{\partial^2}{c^2 \partial t^2}\right) u(t, \boldsymbol{x}) = -\rho(t, \boldsymbol{x}) \tag{1}$$

where c is the speed of light, $u(t, \boldsymbol{x})$ is one component of the electric field and $\rho(t, \boldsymbol{x}) = \psi_{\boldsymbol{x}}(t)\delta(\boldsymbol{x} - \boldsymbol{x}_0)$ is the corresponding source distribution. The solution to (1) is

$$u(t, \boldsymbol{x}) = \int \frac{\rho(t - |\boldsymbol{x} - \boldsymbol{x}'|/c, \boldsymbol{x}')}{4\pi|\boldsymbol{x} - \boldsymbol{x}'|} d\boldsymbol{x}' + \text{noise}. \tag{2}$$

The signals u are then received by a sensor pair ℓ and ℓ' traveling along known flight paths $\boldsymbol{\gamma}_\ell$ and $\boldsymbol{\gamma}_{\ell'}$. Because the waves are traveling at the speed of light, it is appropriate to differentiate between two time scales. As is common in typical active SAR, we call the scale at which the waves propagate *fast time*, and the scale at which the sensors move as *slow time*. Since these time scales are vastly different, we make the "start-stop approximation", in which we assume the sensors are stationary while receiving data. We will denote fast time with the variable t and slow time with the variable s_m or just the index m. Thus the data model becomes, for $\ell = 1, 2$,

$$d^{BB}_{\ell,m}(t) = g_{\ell,m}(\boldsymbol{x}_0) a_{\boldsymbol{x}_0}(t - \tau_{\ell,m}(\boldsymbol{x}_0)) \text{ + noise} \tag{3}$$

where $g_{\ell,m}(\boldsymbol{x}) = G_{\ell,m}(\boldsymbol{x}) e^{-i\omega_0 \tau_{\ell,m}(\boldsymbol{x})}$, $\tau_{\ell,m}(\boldsymbol{x}) = \frac{R_{\ell,m}(\boldsymbol{x})}{c}$, $G_{\ell,m}(\boldsymbol{x}) = (4\pi R_{\ell,m}(\boldsymbol{x}))^{-1}$, and $R_{\ell,m}(\boldsymbol{x}) = |\boldsymbol{x} - \boldsymbol{\gamma}_{\ell,m}|$. Here $a_{\boldsymbol{x}}(t)$ is the complex baseband signal transmitted from location $\boldsymbol{x}$. We assume all clocks are synchronized perfectly and any signals transmitted at carrier frequencies other than $\omega_0 = 2\pi f_0$ are lumped in with the noise term.

The SAPSL approach [11] is to form an image using the following steps.

1) For each hypothesized source location $\boldsymbol{y}$, time-shift the data at each receiver to remove the propagation effects assuming the source is located at $\boldsymbol{y}$. We call this "aligning" the data.
2) Once we align the data, we compute a detection statistic, namely the generalized likelihood ratio, to determine the likelihood that a common signal is present at the different receivers. This likelihood is then plotted as the image value at pixel $\boldsymbol{y}$.
3) We repeat this process for each hypothesized source location $\boldsymbol{y}$.

To carry out step 1, we calculate the time shift at each receiver, assuming the source is at $\boldsymbol{y}$. We then time advance the data to get the aligned data model

$$\eta_{\ell,m}(t, \boldsymbol{y}) = d^{BB}_{\ell,m}(t + \tau_{\ell,m}(\boldsymbol{y})) \text{ + noise.} \tag{4}$$

To derive the detection statistic of step 2, we assume that the noise of (4) is band-limited complex white noise with zero mean and known variance σ_1 and σ_2, respectively. We then formulate two hypotheses, namely H_0, which is that the data consists only of noise, and H_1, which is that the data consists of noise plus an unknown signal, $g_{\ell,m} a_m$, common to the sensors [6]. Here $g_{\ell,m}(\boldsymbol{y})$ is known because $\boldsymbol{y}$ is known. The likelihoods corresponding to H_0 and H_1 are proportional to

$$H_0 : \exp\left(-\sum_m \int \boldsymbol{\eta}_m^\dagger \mathcal{R}^{-1} \boldsymbol{\eta}_m dt \right), \tag{5}$$

$$H_1 : \exp\left(-\sum_m \int (\boldsymbol{\eta}_m - \boldsymbol{g}_m a_m)^\dagger \mathcal{R}^{-1} (\boldsymbol{\eta}_m - \boldsymbol{g}_m a_m) dt \right)$$

where $\mathcal{R} = \text{diag}\{\sigma_1\, \sigma_2\}$ and where we have assembled column vectors $\boldsymbol{\eta}_m = (\eta_{1,m}, \eta_{2,m})^T$ and $\boldsymbol{g}_m = (g_{1,m}, g_{2,m})^T$, with the superscript T denoting transpose. Taking the log of the likelihood ratio, we obtain

$$\mathcal{L}(\boldsymbol{y}) = \sum_m \int (\boldsymbol{\eta}_m - \boldsymbol{g}_m a_m)^\dagger \mathcal{R}^{-1} (\boldsymbol{\eta}_m - \boldsymbol{g}_m a_m) dt - \sum_m \int \boldsymbol{\eta}_m^\dagger \mathcal{R}^{-1} \boldsymbol{\eta}_m dt. \tag{6}$$

Because the waveform $a_{\boldsymbol{y},m}(t)$ is unknown, a maximum likelihood estimate for it is first obtained and then substituted back into (6). After some rearranging [6], [11], we obtain

$$\mathcal{L}(\boldsymbol{y}) = \sum_{\ell,\ell',m} \mathcal{L}_{\ell,\ell',m}(\boldsymbol{y}) \tag{7}$$

where

$$\mathcal{L}_{\ell,\ell',m}(\boldsymbol{y}) \doteq \frac{\overline{g_{\ell,m}(\boldsymbol{y})} g_{\ell',m}(\boldsymbol{y})}{\sigma_\ell^2 \sigma_{\ell'}^2 \sum_{\ell''} |g_{\ell',m}/\sigma_{\ell''}|^2} \langle \eta_{\ell,m}, \eta_{\ell',m} \rangle. \tag{8}$$

More detail can be found in [4], [6], [11].

The detection statistic (7) can be plotted at location $\boldsymbol{y}$ to form an image. We note, however, that the diagonal elements $\mathcal{L}_{\ell,\ell,m}(\boldsymbol{y})$ are merely proportional to the signal energy and thus contain negligible spatial information. Consequently, plotting only the term $\sum_m \mathcal{L}_{1,2,m}(\boldsymbol{y})$ provides equivalent spatial information.

III. Resolution

Even though the imaging formula (8) is clearly nonlinear, it was shown in [11] that resolution, defined in terms of the width of the point spread function, can be characterized in a way similar to what is done in typical (active) SAR. In this section we give a detailed analysis of the resolution, under the start-stop approximation, for two examples of different narrow-aperture sensor geometries, which we call Geometry A and Geometry B.

Geometry A, shown in Fig. 1, consists of one stationary and one moving sensor, with the source located between the two sensors. Geometry B, shown in Fig. 2, consists of two sensors traveling in a straight line, one following the other and the stationary source is offset from the line.

For these cases, we define "range" to be the vertical axis and "cross-range" to be the horizontal axis.

The filtered SAPSL image [11] can be modeled as

$$\mathcal{L}(\boldsymbol{y},\, \boldsymbol{x}) = \int_{\Omega_{\boldsymbol{y}}} e^{i(\boldsymbol{y} - \boldsymbol{x}) \cdot \boldsymbol{k}} d\boldsymbol{k} \tag{9}$$

where $\boldsymbol{y}$ is the hypothesized source location, $\boldsymbol{x}$ is the true source location, and $\boldsymbol{k}$ is a point in $\Omega_{\boldsymbol{y}}$. Details on the derivation of (9) are given in [11]. We refer to the set $\Omega_{\boldsymbol{y}}$ as the *data collection manifold* (DCM); it is determined by the parameters of the sensors and the source. The DCMs for Geometry A and B can be seen in Fig. 3a and 3b. Applying the start-stop approximation to the relevant formulas of [11] shows each point $\boldsymbol{k} \in \Omega_{\boldsymbol{y}}$ can be calculated by

$$\boldsymbol{k} = \omega \nabla \tau_{\ell,\ell',m}(\boldsymbol{y}), \tag{10}$$

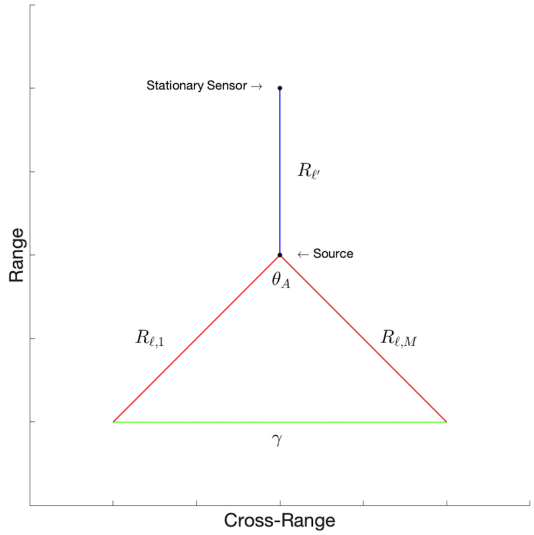

Fig. 1: How angular aperture is defined in Geometry A.

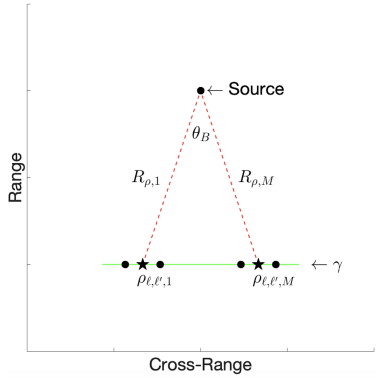

(a) Angular aperture.

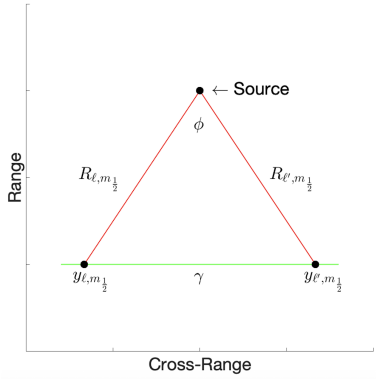

(b) Angle between sensors.

Fig. 2: (a) How angular aperture is defined in Geometry B. The black stars represent the mid-points between the sensors at the circles for slow times 1 and M. (b) How the angle between the sensors is defined.

where

$$\nabla\tau_{\ell,\ell',m}(\boldsymbol{y}) = \frac{\omega\left(\widehat{\boldsymbol{R}}_{\ell,m}(\boldsymbol{y}) - \widehat{\boldsymbol{R}}_{\ell',m}(\boldsymbol{y})\right)}{c} \tag{11}$$

and $\boldsymbol{R}_{\ell,m} = \boldsymbol{y} - \boldsymbol{\gamma}_{\ell,m}$ and $\widehat{\boldsymbol{x}} = \frac{\boldsymbol{x}}{|\boldsymbol{x}|}$. The set $\Omega_{\boldsymbol{y}}$ is determined by the sensor trajectories, the source location, and

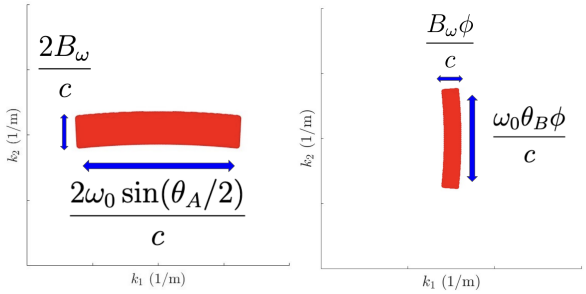

(a) Geometry A (b) Geometry B

Fig. 3: The DCMs for each geometry. The dimensions of the DCM are parameterized by signal characteristics and sensor-source geometry.

the transmitted signal, which we assume to have angular center frequency $\omega_0 = 2\pi f_0$ and angular bandwidth $B_\omega = 2\pi B_f$.

Under the narrow-aperture assumption on the sensor-source geometry, the DCM can be approximated by a rectangle. This is called the rectangular DCM approximation. This allows the integral in equation (9) to be decomposed as the product

$$\begin{aligned}\mathcal{L}(\boldsymbol{y},\boldsymbol{x}) &= \int_{(\Omega_{\boldsymbol{y}})_1} e^{i(y_1-x_1)k_1}dk_1 \int_{(\Omega_{\boldsymbol{y}})_2} e^{i(y_2-x_2)k_2}dk_2, \\ &\propto \operatorname{sinc}\left(\frac{W(y_1-x_1)}{2}\right)\operatorname{sinc}\left(\frac{H(y_2-x_2)}{2}\right),\end{aligned} \tag{12}$$

where $(\Omega_{\boldsymbol{y}})_1$ and $(\Omega_{\boldsymbol{y}})_2$ denote the projection of $\Omega_{\boldsymbol{y}}$ onto the first and second coordinate axes, respectively, and where $\operatorname{diam}((\Omega_{\boldsymbol{y}})_1) = W$ and $\operatorname{diam}((\Omega_{\boldsymbol{y}})_2) = H$. The extents W and H can be calculated by using equations (10) and (11). Below we show how to do this for Geometries A and B.

In this paper, we define resolution as the null-to-null width of the main peak of the sinc functions. These nulls occur when $W(y_1-x_1) = \pm 2\pi$ and $H(y_2-x_2) = \pm 2\pi$. We denote Δy_{CR} and Δy_{R} as cross-range and range resolution, respectively. We can thus calculate resolution as

$$\Delta y_{\text{CR}} = \frac{4\pi}{W} \qquad \text{and} \qquad \Delta y_{\text{R}} = \frac{4\pi}{H}. \tag{13}$$

In the discussion below, we assume the source is located at the origin, so that $\boldsymbol{y} = \boldsymbol{0}$, and drop this notation. Thus $\widehat{\boldsymbol{R}}_{\ell,m} = \widehat{\boldsymbol{R}}_{\ell,m}(\boldsymbol{0})$ etc.

A. *Resolution for Geometry A*

In Geometry A, the unit vector $\widehat{\boldsymbol{R}}_{\ell',m}$, from the stationary sensor to the source will point in the same direction for each slow time m. This is the down pointing blue vector in Fig. 4. In the same figure, we can see that the red unit vectors $\widehat{\boldsymbol{R}}_{\ell,m}$ from the mobile sensor to the source point in the opposite direction of $\widehat{\boldsymbol{R}}_{\ell',m}$. Hence, for the entire narrow aperture (*i.e.,* all m), the vector $\nabla\tau_{\ell,\ell',m}$ will point roughly vertically and will have length approximately $2/c$ for each m. Thus the vertical (range) extent is approximately

$$H = 2B_\omega/c. \tag{14}$$

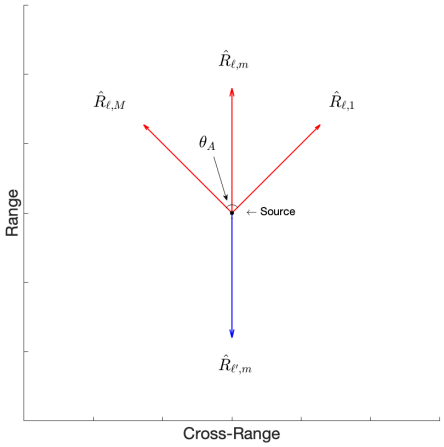

Fig. 4: Unit vectors for Geometry A. The difference of these vectors multiplied by $1/c$ form $\nabla\tau_{\ell,\ell',m}$.

The cross-range (horizontal) extent is determined by the synthetic aperture. In cross-range, we have

$$W = \omega_0 \left| \left(\nabla\tau_{\ell,\ell',1} - \nabla\tau_{\ell,\ell',M} \right)_1 \right|, \tag{15}$$

where the center angular frequency ω_0 is chosen arbitrarily, since the DCM is parametrized by slow-time in cross-range. The slow-time steps $m = 1, M$ are chosen because the angle between these first and last vectors is the aperture angle θ_A. Equation (15) reduces to

$$W = \frac{\omega_0}{c} \left| \left(\widehat{\boldsymbol{R}}_{\ell,M} - \widehat{\boldsymbol{R}}_{\ell,1} \right)_1 \right|. \tag{16}$$

Since the geometry is symmetric, we have $R_{\ell,M} = R_{\ell,1} \doteq R_\ell$. Hence,

$$\left| \left(\widehat{\boldsymbol{R}}_{\ell,M} - \widehat{\boldsymbol{R}}_{\ell,1} \right)_1 \right| = \frac{|\gamma|}{R_\ell}, \tag{17}$$

where $|\gamma|$ represents the length of the mobile path in cross-range. Splitting the equilateral triangle shown in Fig. 1 into two right triangles, we find that each satisfies

$$\sin\left(\frac{\theta_A}{2}\right) = \frac{|\gamma|/2}{R_\ell}, \tag{18}$$

which implies

$$W = 2\frac{\omega_0|\gamma|/2}{cR_\ell} = \frac{2\omega_0}{c}\sin\left(\frac{\theta_A}{2}\right) \approx \frac{\omega_0\theta_A}{c} \tag{19}$$

where we have used the small-angle approximation to obtain the last expression.

Thus from (13), (14), and (19), we obtain the resolution for geometry A as

$$\Delta y_{\text{CR}} = \frac{2c}{f_0\theta_A} \qquad \text{and} \qquad \Delta y_{\text{R}} = \frac{c}{B_f}. \tag{20}$$

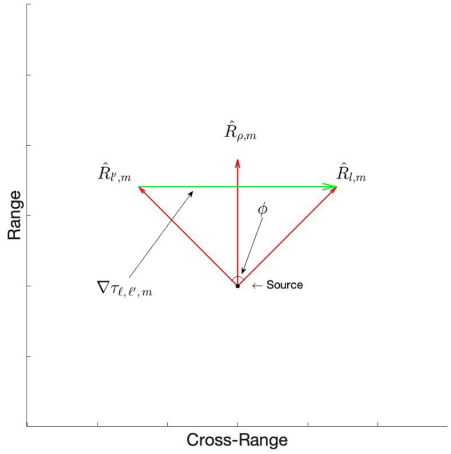

(a) Definition of ϕ.

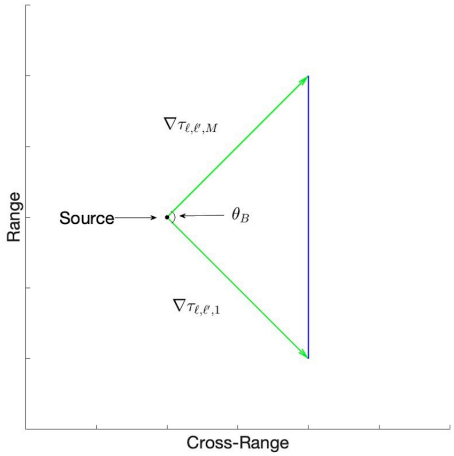

(b) Angle through which $\nabla\tau$ rotates over slow time.

Fig. 5: a) Differences between unit vectors for Geometry B and b) the corresponding TDOA gradients for the first and last looks. The difference of unit vectors from each sensor to the source is a vector pointing to the right in this geometry, which is why the DCM is rotated by $90°$.

B. Resolution for Geometry B

For Geometry B, we see in Fig. 2a that both vectors from the sensors to the source are generally pointing upwards. The corresponding unit vectors, for a fixed sensor location, are shown in Fig. 5a. The difference between these vectors, which is the green vector in Fig. 5a, thus points generally horizontally to the right if sensor ℓ' is to the right of sensor ℓ. When the angle ϕ between the sensors is small, the length of the green vector $\hat{\boldsymbol{R}}_{\ell,m} - \hat{\boldsymbol{R}}_{\ell',m}$ is approximately ϕ (measured in radians) meters. Thus $|\nabla\tau_{\ell,\ell'}| \approx \phi/c$. This means that the horizontal extent W of the DCM is obtained as the interval of $k_1 = \omega|\nabla\tau_{\ell,\ell'}| = \omega\phi/c$, as ω varies over the angular frequency band. Thus

$$W = B_\omega\phi/c = 2\pi B_f\phi/c. \tag{21}$$

The vertical extent of the DCM is obtained from the motion of the sensors. As they move along their trajectory (the green line in Fig. 2), the directions of the unit vectors $\widehat{\boldsymbol{R}}_{\ell,m}$ and $\widehat{\boldsymbol{R}}_{\ell',m}$ rotate. The extent of this rotation is shown

Simulations: Geometry A

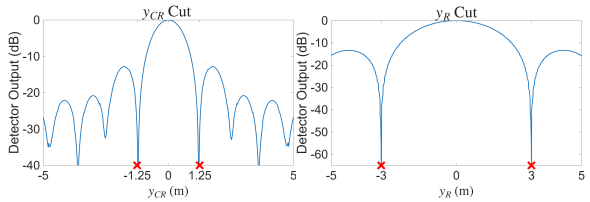

Fig. 6: This figure illustrates that the simulations align with the theoretical formulas derived in this paper. The red markers show where the first nulls should occur based on the theoretical formulas.

Simulations: Geometry B

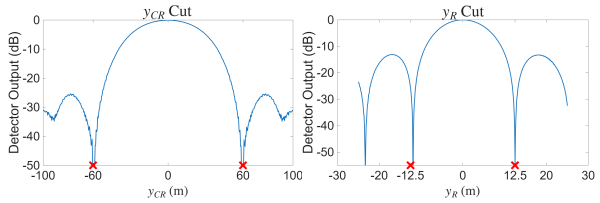

Fig. 7: This figure illustrates that the simulations align with the theoretical formulas derived in this paper. The red markers show where the first nulls should occur based on the theoretical formulas.

in Fig. 5b for the case of sensors moving left to right. Because the trajectory of Fig. 2 subtends an angle θ_B, the vectors $\nabla\tau_{\ell,\ell'} = (\widehat{\boldsymbol{R}}_\ell - \widehat{\boldsymbol{R}}_{\ell'})/c$ (which are approximately perpendicular to $\widehat{\boldsymbol{R}}_\ell$) also move through the angle θ_B. For small angles θ_B, therefore, the vertical extent of the vertical line in Fig. 5b is approximately $\nabla\tau_{\ell,\ell'}\theta_B$. Thus the vertical extent H of the set $\{\boldsymbol{k} \approx \omega_0\nabla\tau_{\ell,\ell',m}\}$, as m varies from 1 to M, is approximately

$$H = \omega_0\phi\,\theta_B/c. \tag{22}$$

With formulas (13), (21), and (22), we obtain the Geometry B resolution

$$\Delta y_{\text{CR}} = \frac{2c}{B_f\phi} \qquad \text{and} \qquad \Delta y_{\text{R}} = \frac{2c}{f_0\theta_B\phi}. \tag{23}$$

IV. Numerical Simulations

We ran simulations to provide numerical support for the theoretical resolution formulas. For both geometries, a chirp signal with bandwidth 50 MHz was used as the transmitted signal. The mobile sensor(s) created an aperture of 0.1 radians. The formulas predict $\Delta y_{CR} \approx 2.5$m and $\Delta y_R \approx 6$m for Geometry A while $\Delta y_{CR} \approx 120$m and $\Delta y_R \approx 25$m for Geometry B. Fig. 6 and 7 show that the simulations confirm the theoretical formulas for both Geometry A and B, respectively. The red x's in the images are plotted where the first nulls should be.

V. Conclusions

In this article we have derived resolution formulas for the Synthetic Aperture Passive Source Localization (SAPSL) algorithm for two geometries of interest. We consider only the case of slowly moving sensors and narrow angular apertures. Here resolution is defined as the null-to-null width of the point spread function (PSF) of the SAPSL method. The width of the PSF is determined by the dimensions of the set of spatial Fourier components. We have shown that the dimensions of this set depend on the angular extent of the sensor-source geometry and on the characteristics of the emitted signal.

We also provided numerical simulations that verify the resolution predicted from the formulas.

Acknowledgment

This work was supported in part by the Office of Naval Research under contract N000142412241 and by the Air Force Office of Scientific Research under the contract FA9550-24-1-0151. We are grateful to Charles Dietlein, Jonathan Chisum, and Michael Baram for many helpful discussions.

References

[1] B. Himed D. E. Hack, L. K. Patton. A unified detection framework for distributed active and passive RF sensing. In *2013 Asilomar Conf. on Signals, Systems, and Computers (IEEE)*, pages 449–453. IEEE, 2003.

[2] S. Kay N. Vankayalapati. Asymptotically optimal detection of low probability of intercept signals using distributed sensors. *IEEE*, 48:737–748, 2012.

[3] M. Cheney L. T. McWhorter, L. Scharf. First-order statistical framework for multi-channel passive detection. *arXiv preprint arXiv:2302.06816*, 2023.

[4] J. A. Given M. Cheney L. Scharf, L. T. McWhorter. General first-order framework for passive detection with two sensor arrays. In *2019 53rd Asilomar Conf. on Signals, Systems, and Computers (IEEE)*, pages 94–97. IEEE, 2019.

[5] A. J. Weiss. Direct position determination of narrowband radio frequency transmitters. *IEEE Signal Process. Lett.*, 11:513–516, 2004.

[6] C. Moore M. Cheney L. T. McWhorter, L. Scharf. Passive multi-channel detection: A general first-order statistical theory. *IEEE*, 4:437–451, 2023.

[7] Y. T. Chan K. C. Ho. Geolocation of a known altitude object from TDOA and FDOA measurements. *IEEE*, 33:770–783, 1997.

[8] A. J. Weiss A. Amar. Direct position determination: a single-step emitter localization approach. *Classical and Modern Direction-of-Arrival Estimation (Elsevier)*, pages 385–424, 2009.

[9] J. A. Given C. Waddington, M. Cheney. Synthetic aperture source localization. *Inverse Problems (IOP Publishing)*, 36(1):015007, 2019.

[10] A. Waddington. *Synthetic Aperture Source Localization*. PhD thesis, Colorado State University, 2018.

[11] M. Rhilinger C. Moore A. Celestin M. Cheney, L. Scharf. Image analysis and resolution for detection-based synthetic-aperture passive source localization. *Inverse Problems (IOP Publishing)*, 40(5):055003, 2024.